Dalton Transactions

Accepted Manuscript

This article can be cited before page numbers have been issued, to do this please use: E. A. Zvereva, M. I. Stratan, A. Ushakov, V. B. Nalbandyan, I. Shukaev, A. V. Silhanek, M. Abdel-Hafiez , S. Streltsov and A. N. Vasiliev, *Dalton Trans.*, 2016, DOI: 10.1039/C6DT00516K.

ROYAL SOCIETY OF CHEMISTRY

www.rsc.org/dalton

View Article Online
DOI: 10.1039/C6DT00516K

Journal Name

ARTICLE

HPSTAR 178-2016

Orbitally induced hierarchy of exchange interactions in zigzag antiferromagnetic state of honeycomb silver delafossite $Ag_3Co_2SbO_6$

Received 00th January 20xx,
Accepted 00th January 20xx

DOI: 10.1039/x0xx00000x

www.rsc.org/

E.A. Zvereva,[a,*] M.I. Stratan,[a] A.V. Ushakov,[b] V.B. Nalbandyan,[c] I.L. Shukaev,[c] A.V. Silhanek,[d] M. Abdel-Hafiez,[e,f,g] S.V. Streltsov,[b,h] and A.N. Vasiliev[a,h,i]

We report the revised crystal structure, static and dynamic magnetic properties of quasi-two dimensional honeycomb-lattice silver delafossite $Ag_3Co_2SbO_6$. The magnetic susceptibility and specific heat data are consistent with the onset of antiferromagnetic long range order at low temperatures with Néel temperature T_N ~ 21.2 K. In addition, the magnetization curves revealed a field-induced (spin-flop type) transition below T_N in moderate magnetic fields. The GGA+U calculations show the importance of the orbital degrees of freedom, which maintain a hierarchy of exchange interaction in the system. The strongest antiferromagnetic exchange coupling was found in the shortest Co-Co pairs and is due to direct and superexchange interaction between the half-filled *xz+yz* orbitals pointing directly to each other. The other four out of six nearest neighbor exchanges within the cobalt hexagon are suppressed, since for these bonds active half-filled orbitals turned out to be parallel and do not overlap. The electron spin resonance (ESR) spectra reveal a broad absorption line attributed to Co^{2+} ion in octahedral coordination with average effective g-factor g=2.40±0.05 at room temperature and show strong divergence of ESR parameters below ~ 150 K, which implies an extended region of short-range correlations. Based on the results of magnetic and thermodynamic studies in applied fields, we propose the magnetic phase diagram for the new honeycomb-lattice delafossite.

Introduction

Delafossite compounds are one of the largest families of oxides attracting a lot of attention both due to remarkable variety of their physical properties and numerous applications as catalysts, multiferroics, thermolelectric and luminescent materials, battery cathodes, transparent conductors for solar cell technologies, etc. The most studied family is AMO2 oxides, where the monovalent A-site cations (Ag+, Cu+, Pd+, or Pt+) adopt linear coordination, while the M-site cation (transition metal, Al, Ga, etc) is octahedrally coordinated by oxygen and forms a triangular lattice.[1] Geometrical frustration triggered by the triangular network in presence of antiferromagnetic interactions leads to many fascinating phenomena discovered in the delafossite compounds. In particular, spectacular examples of a multiferroic behavior, the coexistence of magnetic order and ferroelectricity was found in different compounds with delafossite or closely related structures: $ACrO_2$ (A = Cu, Ag),[2-4] $AgFeO_2$,[5,6] $CuFeO_2$,[7,8] $CuFe_{1-x}M_xO_2$ (M = Al, Ga),[9-11] and $AgCrS_2$.[12-13] Unusual spin dynamics in agreement with the Z_2-vortex ordering scenario was revealed for $ACrO_2$ (A = Cu, Ag, Pd)[14] and a very strong doping dependence of the magnetic properties was found in $CuMnO_2$.[15-16] Remarkable phenomenon of dimensional crossover from anisotropic 3D (antiferromagnetic) to 2D low-energy magnetic excitations (spin-liquid like state) was found in delafossite oxide $Cu_{1-x}Ag_xCrO_2$ with an increase of x.[17]

The honeycomb lattice is also a variant of structure with triangular geometry and can also be magnetically frustrated due to the next nearest neighbour interactions. As it was shown theoretically, quantum fluctuations may stabilize a quantum spin liquid (SL) phase between a state of massless Dirac fermions and an antiferromagnetically ordered insulating phase.[18] Moreover, many other exotic phases may appear in the system with the honeycomb lattice: an unusual Z_2 SL state, phase with quasi-molecular orbitals formed on the hexagons, incommensurate Néel order, a dimerized state with spontaneously broken rotational symmetry, a valence bond liquid and lattice nematic phases, columnar dimer order with a non-bipartite structure, etc.[19-30]

In contrast to the triangular lattice delafossites mentioned above, investigations of magnetic properties for the honeycomb lattice counterparts started very recently. One can

[a] Faculty of Physics, Moscow State University, 119991 Moscow, Russia
zvereva@mig.phys.msu.ru
[b] Institute of Metal Physics, S. Kovalevskoy St. 18, 620990 Ekaterinburg, Russia
[c] Chemistry Faculty, Southern Federal University, 344090 Rostov-on-Don, Russia
[d] Département de Physique, Université de Liége, B-4000 Sart Tilman, Belgium
[e] Institute of Physics, Goethe University Frankfurt, 60438 Frankfurt/M, Germany
[f] Faculty of Science, Physics Department, Fayoum University, 63514 Fayoum, Egypt
[g] Center for High Pressure Science & Technology Advanced Research, 1690 Cailun Rd, Shanghai, 201203, P.R. China
[h] Ural Federal University, 620002 Ekaterinburg, Russia
[i] National University of Science and Technology "MISiS", 119049 Moscow, Russia

†Electronic Supplementary Information (ESI) available on rsc.org: a commented list of all known $Ag_3M_2RO_6$ and Ag_3MRXO_6 delafossites and refinement results for $Ag_3M_2SbO_6$ (M = Co, Zn) (pdf) and crystallographic information files (cif) for $Ag_3M_2SbO_6$ (M = Co, Zn) See DOI: 10.1039/x0xx00000x

View Article Online
DOI: 10.1039/C6DT00516K

expect that simple geometrical frustration will be removed on honeycomb lattice; however, non-trivial quantum ground states might be realized due to frustrating second and third neighbor interactions. In particular, among the $Cu_3M^{2+}{}_2SbO_6$ series (M = Mn, Co, Ni, Cu), the magnetism of manganese compound was not characterized at all.[31] The honeycomb S=1/2 delafossite compound Cu_5SbO_6 ($Cu^+{}_3Cu^{2+}{}_2Sb^{5+}O_6$) was characterized as dimerized system, in which the ground state is a spin singlet[32] similarly to previously known $NaFeO_2$-derived Cu^{2+} honeycomb compounds $Na_2Cu_2TeO_6$[33-35] and $Na_3Cu_2SbO_6$[35-39] and in spite of significant structural differences. At the same time both polytypes of $Cu_3Ni_2SbO_6$ and $Cu_3Co_2SbO_6$ compounds were found to order antiferromagnetically with transitions, at 22.3 and 18.5 K for Ni and Co variants, respectively, with Curie−Weiss fits that are in agreement with Ni^{2+} and Co^{2+} high spins.[40,41] The magnetic structures of these monoclinic polytypes were determined by neutron diffraction at 4 K and described as ferromagnetic chains running along the *b*-direction which are antiferromagnetically coupled, resulting in an overall antiferromagnetic "zigzag" ordering in the honeycomb plane. The magnetic **q** vector is [100] for both materials; however, the moments are aligned along the *b*-axis for the Co based compounds while for the Ni sample they are in the *ac* - plane.

In the family of silver delafossites, 19 superstructures are known now,[31,42-53] although structural characterization for 18 of them is incomplete or doubtful due to stacking faults (for details, see Table S1 of the Electronic Supplementary Information (ESI)). Of these 19, seven are non-magnetic, six are $Ag_3M_2XO_6$ type with apparently honeycomb arrangement of the magnetic M cations, and the remaining six are Ag_3MRXO_6 type with halved content of the magnetic M cations and, thus, MO_6 octahedra apparently isolated from each other. Of these 12 phases with magnetic cations, no physical characterization has been performed for $Ag_3Ni_2SbO_6$,[31] $Ag_3Co_2SbO_6$,[46] $Ag_3Ni_2BiO_6$,[50] $Ag_3(NaFeSb)O_6$,[51] $Ag_3(LiMTe)O_6$ (M^{2+} = Co, Ni)[52] and $Ag_3(LiMSb)O_6$ (M^{3+} = Cr, Mn, Fe).[53] The delafossite $Ag_3LiRu_2O_6$ was declared as a promising candidate for thermoelectric applications due to the combination of two-dimensionality, good conductivity and stacking disorder that is likely to correlate with low thermal conductivity.[47] Basic magnetic and transport characterization was also performed for $Ag_3LiM_2O_6$ (M = Rh, Ir)[49] and the low-spin configurations of $4d^5$ and $5d^5$ ions were supposed from analysis of magnetic response in the paramagnetic phase.

In the present work we performed detailed revision of the crystal structure of the quasi-2D honeycomb-lattice oxide $Ag_3Co_2SbO_6$ and its static and dynamic magnetic properties were thoroughly investigated for the first time aiming to determine its quantum ground state, magnetic structure and to build the magnetic phase diagram.

Experimental and calculation details

Ion-exchange preparation of $Ag_3Co_2SbO_6$ from $Na_3Co_2SbO_6$, its chemical and X-ray diffraction (XRD) analysis were described earlier.[46] The sample $Ag_3Zn_2SbO_6$ used here as a diamagnetic analogue for specific heat measurements, was prepared in a similar way from the lithium precursor. Completeness of the substitution was confirmed by the chemical analysis: 49,1 weight % Ag found, 48,2 % calculated. XRD powder analysis was performed with an ARL X'TRA diffractometer equipped with a solid-state Si(Li) detector using CuK_α radiation. The powder patterns of the two compounds (Figs. 1 and 2) are almost indistinguishable. The Rietveld refinements were performed using the GSAS+EXPGUI suite.[54,55]

The magnetic measurements were performed by means of a Quantum Design SQUID – magnetometer. The temperature dependence of magnetic susceptibility was measured at the magnetic field B = 0.1 T in the temperature range 1.8–300 K. The isothermal magnetization curves were obtained for magnetic fields $B \le 5$ T at T = 1.8, 2, 2.5, 3, 5, 8, 15, 20, 30 K after cooling the sample in zero field.

The specific heat measurements were carried out by a relaxation method using a Quantum Design PPMS system. The plate-shaped samples of $Ag_3Co_2SbO_6$ of ~0.2 mm thickness and 14.13 mg mass and $Ag_3Zn_2SbO_6$ of ~0.2 mm thickness and

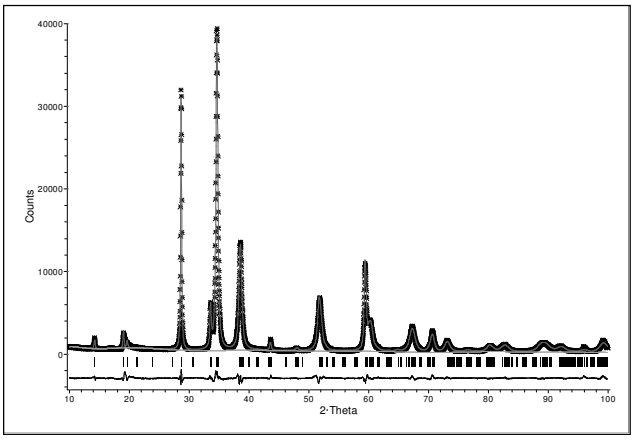

Fig. 1 XRD profile of $Ag_3Co_2SbO_6$. Stars – experimental data, dark gray line – calculated pattern, light gray line – background, vertical bars – Bragg ticks, thin black line below – difference.

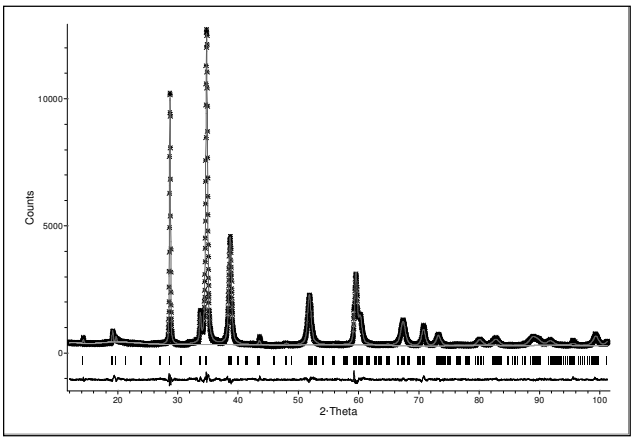

Fig. 2 XRD profile of $Ag_3Zn_2SbO_6$. Stars – experimental data, dark gray line – calculated pattern, light gray line – background, vertical bars – Bragg ticks, thin black line below – difference.

DOI: 10.1039/C6DT00516K

9.62 mg mass were obtained by cold pressing of the polycrystalline powder. Data were collected at zero magnetic field and under applied fields up to 9 T in the temperature range 2 – 300 K.

Electron spin resonance (ESR) studies were carried out using an X-band ESR spectrometer CMS 8400 (ADANI) ($f \approx 9.4$ GHz, $B \leq 0.7$ T) equipped with a low-temperature mount, operating in the range $T = 6$–270 K. The effective g-factors of our samples have been calculated with respect to an external reference for the resonance field. We used BDPA (a,g - bisdiphenylene-b-phenylallyl) $g_{ref} = 2.00359$, as a reference.

The band structure calculation were carried out within the GGA+U approximation[56] using full-potential linearized augmented plane wave (FP-LAPW) method as realized in the Wien2k code.[57] The exchange-correlation potential was taken in the form proposed by Perdew, Burke and Ernzerhof.[58] We chose the on-site Coulomb repulsion parameter for Co to be U = 7 eV, while Hund's rule coupling parameter (JH) was taken as $J_H = 0.9$ eV.[59,60] The spin-orbit coupling for the valence shells was not taken into account in the present calculations. The Brillouin-zone (BZ) integration in the course of the self-consistency iterations was performed over 12x10x12 mesh in *k*-space. The parameter of the plane wave expansion was chosen to be $R_{MT}K_{max} = 7$, where R_{MT} is the smallest muffin-tin sphere radii and K_{max} - plane wave cut-off. The muffin-tin radii equal to 2.05, 1.72, 2.04 and 1.72 Bohr for Co, Sb, Ag, and O, respectively. The exchange integrals *J* were calculated by fitting the total energy difference of four magnetic configurations to the Heisenberg model written as

$$H = \sum_{ij} J_{ij} \vec{S}_i \vec{S}_j \quad , \qquad (1)$$

i.e. each pair in Eq. (1) was counted twice.

Results and discussion

Structural description

Initially, the laboratory XRD data of $Ag_3Co_2SbO_6$ and its sodium precursor were interpreted in trigonal system (space group $P3_112$) since no peak splitting indicative of symmetry lowering could be observed.[46] Nevertheless, crystal structure of $Na_3Co_2SbO_6$ was refined in the monoclinic space group C2/m.[61] Recently, using high-resolution synchrotron data, we definitely confirmed peak splitting and monoclinic symmetry for $Na_3Co_2SbO_6$, similar to $Li_3Zn_2SbO_6$[62] and $Li_3Ni_2SbO_6$.[63] This suggested that the structure of $Ag_3Co_2SbO_6$ may also be monoclinic. The C2/m model, although less symmetrical in the unit cell data (four lattice parameters vs. two for the trigonal cell), seems to be more symmetrical in the atomic structure, having only seven variable atomic coordinates vs. fifteen coordinates in the $P3_112$ model. Therefore, we attempted here a revision of the crystal structure of $Ag_3Co_2SbO_6$ on the C2/m model using the same experimental XRD profile.

Polyhedral view of obtained C2/m crystal structure of $Ag_3Co_2SbO_6$ is presented in Fig. 3(a). Note that both models

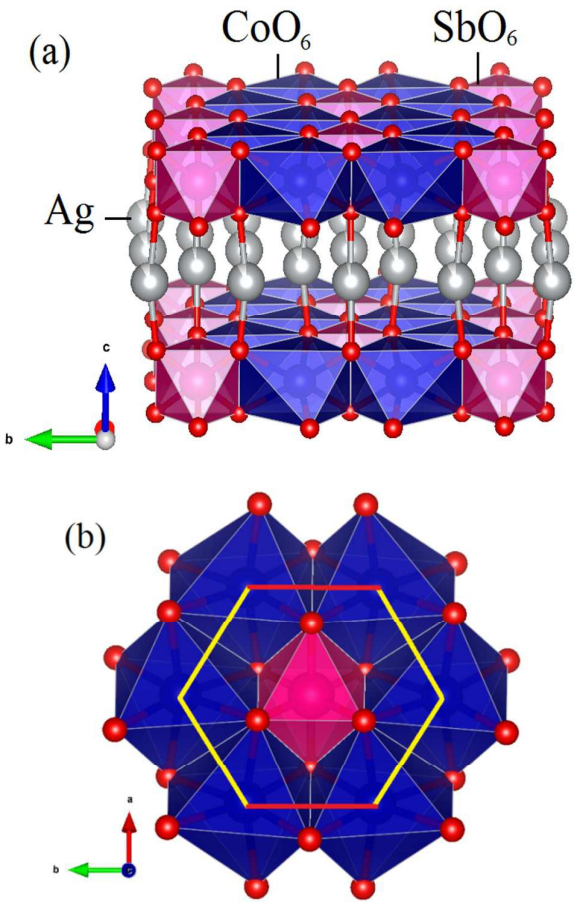

Fig. 3 Polyhedral view of a layered C2/m crystal structure of $Ag_3Co_2SbO_6$ (a) and its fragment within the magneto-active layers, assuming complete cation ordering (ignoring fictitious Co/Sb mixing) (b). CoO_6 and SbO_6 octahedra are shown by blue and pink color, respectively. Silver and oxygen ions are gray and red spheres, respectively. Long and short Co-Co distances are denoted by yellow and red lines, respectively.

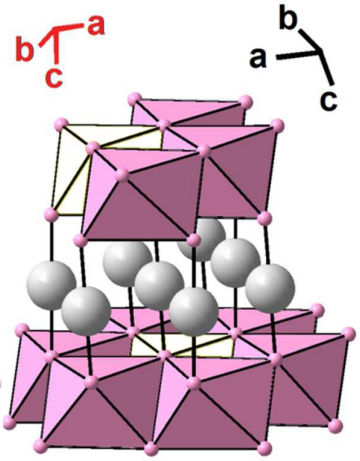

Fig. 4 Two adjacent layers in $Ag_3Co_2SbO_6$, similar arrangement of the two structural models: P3112 and C2/m, with corresponding coordinate systems on left and right, respectively. SbO_6 and CoO_6 octahedra are white and pink, respectively, and silver ions are shown as gray balls.

View Article Online
DOI: 10.1039/C6DT00516K

($P3_112$ and C2/m) have essentially identical honeycomb $[Co_2SbO_6]^{3-}$ layers (Fig. 3(b)) and dumbbell coordination of the interlayer Ag^+, but differ in the layer stacking mode. However, mutual positions of the two adjacent octahedral layers is the same in the two structures (Fig. 4) and the difference only becomes obvious when the third layer is added. The same holds for the two models for $Na_3M_2SbO_6$, although sodium coordination is octahedral rather than linear. This enables formation of multiple stacking faults, especially characteristic for silver compounds due to (i) larger interlayer distances (e.g., 5.36 Å for $Na_3Co_2SbO_6$ and 6.22 Å for $Ag_3Co_2SbO_6$) and (ii) layer gliding during the ion exchange driving cation coordination from octahedral to linear.

Due to multiple stacking faults, the monoclinic phases effectively imitate trigonal symmetry, and their superlattice reflections responsible for M^{2+}/Sb^{5+} ordering are anomalously diffuse and weak for both Co^{2+} and Zn^{2+} compounds (Figs. 1 and 2). This is a typical feature of other compounds of this class listed in Table S1 of the ESI. This feature hinders their structural investigation. None of the 18 silver delafossite superstructures listed in Table S1, prepared by ion exchange, could receive adequate structural description. Note that $Ag_3Zn_2SbO_6$ was prepared earlier from the same precursor but no superlattice effects were observed although the authors anticipated them[31] and the starting $Li_3Zn_2SbO_6$ showed unambiguous Zn/Sb ordering.[62]

Results of our structural refinements for both Co^{2+} and Zn^{2+} compounds are shown in Figs. 1 and 2 and listed in Tables S2, S3 and S4 of the ESI and in Crystallographic information files (cif). Reasonable agreement between experimental and calculated profiles could only be obtained with considerable M^{2+}/Sb^{5+} mixing on octahedral positions. However, we suppose that this substitution is only fictitious due to stacking faults, and each individual layer is essentially ordered as in many other similar superstructures.[41,47,48,64-67] Note that average metal-oxygen distances for nominal ($Sb_{0.46}Co_{0.54}$) and ($Co_{0.73}Sb_{0.27}$) sites, 1.88 and 2.21 Å, respectively, differ significantly and do not support mixing, since ionic radii sums for Sb^{5+}-O and Co^{2+}-O bonds are 1.98 and 2.12 Å, respectively. The Co and Zn compounds are strictly isostructural and even have very similar degree of the apparent M^{2+}/Sb^{5+} substitution. The polyhedral view of the $Ag_3Co_2SbO_6$ crystal structure, ignoring this mixing, is shown in Figs. 3-4. The refined silver site occupancies in $Ag_3Co_2SbO_6$ are slightly lower than unity in accordance with the analytical data: 47.3 % Ag found,[46] 49.3% calculated from the ideal formula.

Magnetic susceptibility and magnetization

The temperature dependence of magnetic susceptibility $\chi(T)$ implies an antiferromagnetic behaviour. It was established, that upon a decrease of the temperature the $\chi(T)$ dependence at the field B = 0.1 T passes through a sharp maximum at T_{max} ~ 25.2 K and then drops (Fig. 5(a)). Such behaviour indicates an onset of antiferromagnetic long-range ordering in the material at low temperature. The $\chi(T)$ dependence recorded upon cooling the sample in zero

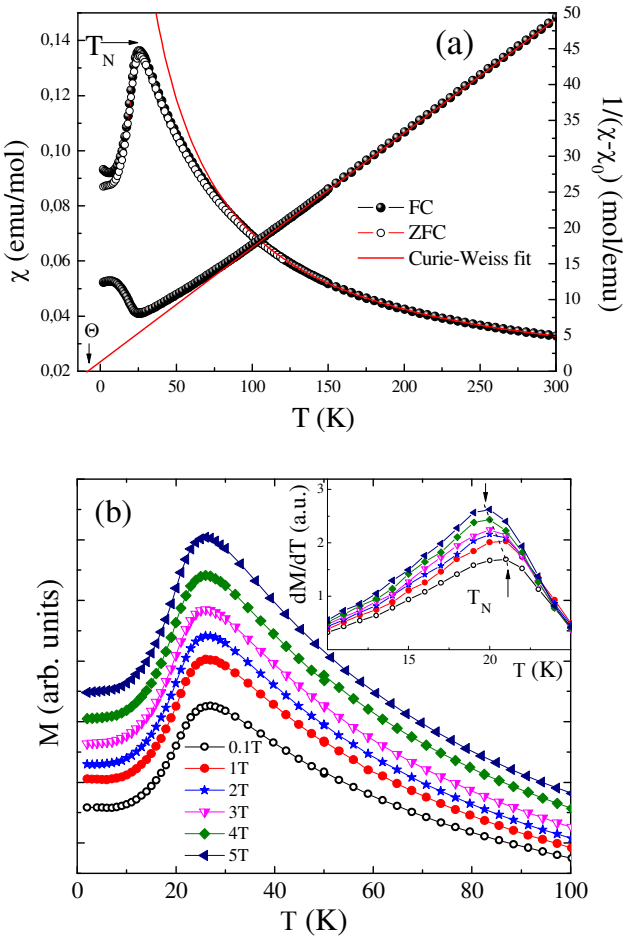

Fig. 5 (a) Temperature dependence of the magnetic susceptibility recorded in ZFC (open circles) and FC (filled circles) regimes at B = 0.1 T for $Ag_3Co_2SbO_6$. The solid curve represents an approximation in accordance with the Curie-Weiss law. (b) M(T) curves at various external magnetic fields. On inset: the derivative curves highlighting the slight shift of T_N upon variation of the magnetic field.

magnetic field (ZFC) mode and in magnetic field (FC) one shows practically no divergence down to ~7 K. In applied magnetic fields the position of the T_{max} is slightly shifted to the low temperature side (Fig. 5(b)).

At high temperatures, the magnetic susceptibility nicely follows the Curie-Weiss law with addition of a temperature-independent term χ_0 The best fit of the experimental data in the range 200-300 K yields χ_0 = 0.012(3) emu/mol, C = 5.7(5) emu/mol K and the Weiss temperature Θ = -9(1) K indicating a predominance of the antiferromagnetic interaction in the compound. The effective magnetic moment μ_{eff} as estimated from the Curie constant is 6.7 μ_B/f.u., which agrees with one expected from theoretical estimations for system of two high spin (HS) Co^{2+} ions per formula unit obtained by using g = 2.4 experimentally determined from the ESR spectra (see below).

The full magnetization isotherm $M(B)$ at T = 1.8 K for $Ag_3Co_2SbO_6$ shows no hysteresis and no saturation in magnetic fields up to 5 T (Fig. 6). It is worth noting, that within this range

View Article Online
DOI: 10.1039/C6DT00516K
Journal Name ARTICLE

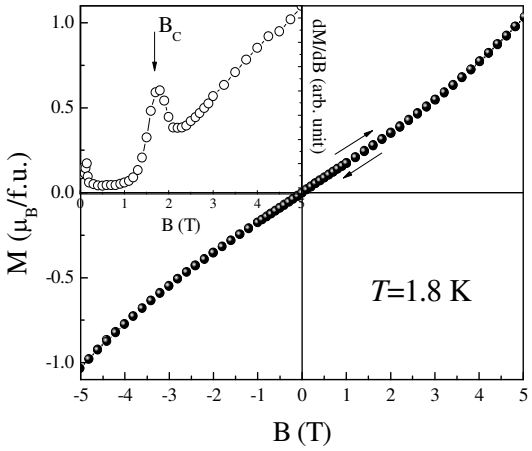

Fig. 6 The full magnetization isotherm for $Ag_3Co_2SbO_6$ and its first derivative dM/dB (on inset) at T=1.8 K.

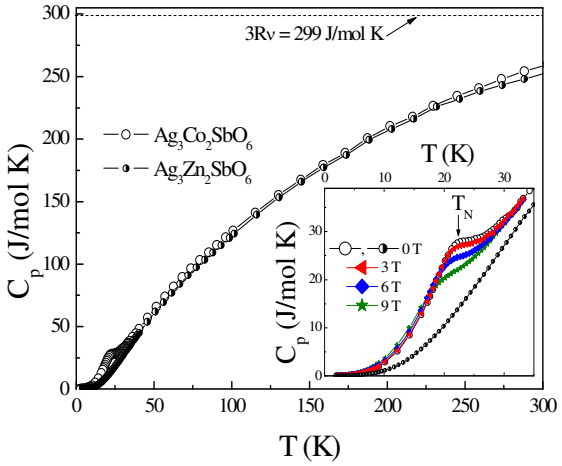

Fig. 7 Temperature dependence of the specific heat in Ag3Co2SbO6 (black open circles) and the isostructural diamagnetic compound Ag3Zn2SbO6 (black half-filled circles) in zero magnetic field. Inset: enlarged low temperature part highlights the onset of antiferromagnetic spin ordering and shift of the TN in magnetic fields.

of the applied magnetic fields, the magnetic moment is still below the theoretically expected saturation magnetic moment for two Co^{2+} ions per formula unit assuming either high-spin (S=3/2) or low-spin state (S=1/2): $M_{sat} = 2gS\mu_B$. One can see, however, that the magnetization curve has a slight upward curvature suggesting the presence of a magnetic field induced spin-flop type transition. The value of critical field has been estimated from the maximum in the derivative d*M*/d*B*(*B*) curve as high as B_C ~ 1.9 T (see an inset in Fig. 6). With increasing temperature, the amplitude of this anomaly decreases rapidly, and the feature becomes undetectable above T_N (Fig. S1 of the ESI). It is worth to mention that the spin-reorientation-type transitions have been reported recently for several related antimonates: for example, $Na_3Co_2SbO_6$,[61] $Li_3Ni_2SbO_6$,[63] $Na_3Ni_2SbO_6$,[76] Li_4FeSbO_6.[67]

Specific heat

The specific heat data *C*(*T*) for $Ag_3Co_2SbO_6$ at zero magnetic field are in good agreement with the temperature dependence of magnetic susceptibility in weak magnetic fields, and demonstrate a distinct λ-shaped anomaly, which is characteristic of a three-dimensional (3D) magnetic order (Fig. 7). Note, however, that the absolute value of the Néel temperature T_N ~ 21.2 K, deduced from *C*(*T*) data at *B* = 0 T is slightly lower than T_{max} ~ 25.2 K on χ(T) dependence at *B* = 0.1 T (Fig. 5), whereas it correlates with a maximum on the magnetic susceptibility derivative dχ/d*T*(*T*). Indeed, as it has been shown by Fisher [68,69] the temperature dependence of the specific heat *C*(*T*) for the antiferrimagnets with short-range interactions should follow the derivative of the magnetic susceptibility in accordance with:

$$C(T) = A\left(\partial/\partial T\right)\left[T\chi_{\parallel}(T)\right], \quad (1)$$

where the constant *A* depends weakly on temperature. In accordance with Eq. (2), the λ-type-anomalies observed in *C*(*T*) dependence at the antiferromagnetic transition temperature are defined by an infinite positive gradient on the curve $\chi_{||}(T)$ at TN, while a maximum $\chi_{||}(T)$ lies usually slightly above the ordering temperature. Thus, the anomaly in the specific heat should correspond to the similar anomaly in $d\chi_{||}/dT(T)$.[70]

In order to analyze the nature of the magnetic phase transition and to evaluate the corresponding contribution to the specific heat capacity and entropy, specific heat was also measured for the strictly isostructural diamagnetic material $Ag_3Zn_2SbO_6$. The specific heat data for both magnetic and diamagnetic samples in the *T*-range 2-300 K are shown in Fig. 7. The Dulong-Petit value reaches 3Rz = 299 J/mol K, with the number of atoms per formula unit z = 12. We observe a specific heat jump of ΔC_p ~ 14.4 J/mol K at T_N, which is a noticeably smaller than the value expected from the mean-field theory for the antiferromagnetic ordering of two Co^{2+} ions system assuming all ions to be in the high-spin (S=3/2) state:[71]

$$\Delta C_p = 5R\frac{2S(S+1)}{S^2+(S+1)^2} \approx 36.7 \text{ J/mol×K} \quad (2)$$

where R being the gas constant R=8.31 J/mol K. Note, that such a reduction of ΔC_p may indicate the presence of strong short-range magnetic correlations at higher temperature in $Ag_3Co_2SbO_6$. In applied magnetic fields, the T_N - anomaly is slightly rounded and markedly shifts to the lower temperature (see inset in Fig. 7).

For quantitative estimations we assume that the specific heat of the isostructural compound $Ag_3Zn_2SbO_6$ provides a proper estimation for the pure lattice contribution to specific heat. In the frame of Debye model the phonon specific heat is described by the function:[71]

View Article Online
DOI: 10.1039/C6DT00516K

$$C_{ph} = 9R\left(\frac{T}{\theta_D}\right)^3 \int_0^{T/\theta_D} \frac{e^x x^4}{\left(e^x - 1\right)^2} dx \quad , \qquad (3)$$

where $x = \hbar\omega/kT$, $\Theta_D = \hbar\omega_{max}/k$ is Debye temperature, ω_{max} is maximum frequency of the phonon spectrum, k is Boltzmann constant. The value of Debye temperature Θ_D estimated from approximation of $C(T)$ according to this T^3 – law in low temperature range for the diamagnetic compound $Ag_3Zn_2SbO_6$ was found to be about ~ 285 ± 5 K. Normalization of the Debye temperatures has been made taking into account the difference between the molar masses for Zn – Co atoms in the $Ag_3Co_2SbO_6$ compound resulting in Θ_D ~ 286 ± 5 K.

The magnetic contribution to the specific heat was determined by subtracting the lattice contribution using the data for the isostructural non-magnetic analogue (Fig. 8). We examine the $C_m(T)$ below T_N in terms of the spin-wave (SW) approach assuming the limiting low-temperature behavior of the magnetic specific heat should follow $C_m \sim T^{d/n}$ - power law for magnons,[66] where d stands for the dimensionality of the magnetic lattice and n is defined as the exponent in the dispersion relation $\omega \sim \kappa^n$. For antiferromagnetic (AFM) and ferromagnetic (FM) magnons $n = 1$ and $n = 2$, respectively. The least square fitting of the data below T_N (upper panel in Fig. 8) has given with good accuracy $d = 3$ and $n = 0.9$ values, that corroborates the picture of 3D AFM magnons at the low temperatures.

The entropy change has been calculated using the equation:

$$\Delta S_m(T) = \int_0^T \frac{C_m(T)}{T} dT$$

One can see that the magnetic entropy ΔS_m saturates at about 40 K, reaching approximately 9.6 J/mol K (lower panel in Fig. 8). This value is essentially lower than the magnetic entropy change expected from the mean-field theory for system of two cobalt magnetic ions with S=3/2 per formula unit: $\Delta S_m = 2R\ln(2S+1) \approx 23$ J/(mol K). One should note that the magnetic entropy released below T_N removes only about 26% of the saturation value. This indicates the presence of appreciable short-range correlations far above T_N, which is usually characteristic feature for materials with lower magnetic dimensionality.[70]

ESR spectra

Over the whole temperature range studied the ESR powder pattern is dominated by a broad overlapping in nature absorption line, which can be attributed to Co^{2+} ions in distorted octahedral coordination. No hyperfine structure arising from an electron-nucleus interaction for the ^{59}Co isotope (100% abundance, $I = 7/2$) is observed in the spectrum, presumably due to the large linewidth, which could mask the bandwidth of absorption of the powder sample considered without the natural broadening. The amplitude of signal

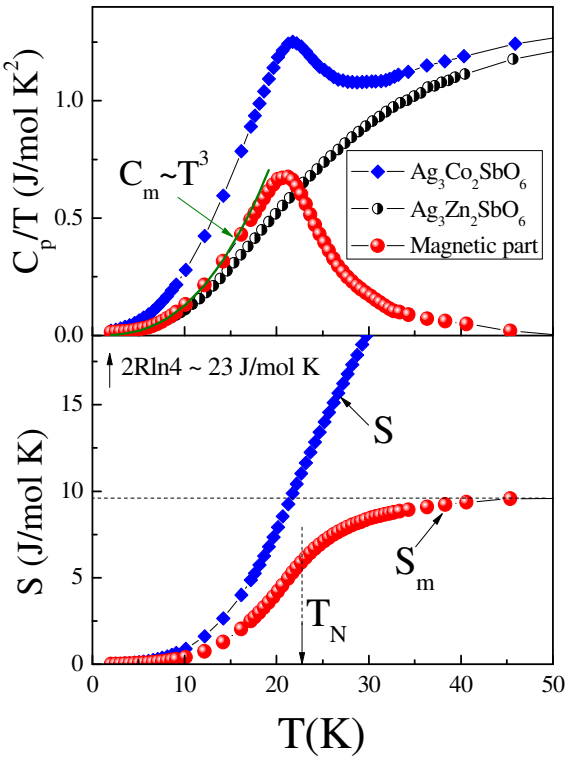

Fig. 8 Magnetic specific heat (red filled circles on upper panel) and magnetic entropy (red filled circles on lower panel) in comparison with the specific heat data for $Ag_3Co_2SbO_6$ (blue diamonds) and non-magnetic analogue $Ag_3Zn_2SbO_6$ (black half-filled circles) at B = 0 T. Solid curve indicates the spin wave contribution estimated in accordance with $C_m \sim T^{d/n}$ - power law for magnons.

increases monotonously upon cooling the sample, then the signal weakens in amplitude and eventually in the vicinity of T_N its degradation occurs, which is indicative of the opening of a spin gap for the resonance excitation due to the onset of long range magnetic order at low temperatures.

Overlapping asymmetric character of the lineshape may indicate anisotropy of the effective g-tensor since monoclinic crystal structure of $Ag_3Co_2SbO_6$, described above, presumes only one crystallographic position for the Co^{2+} ions in octahedral coordination (Fig. 3). For a S = 3/2 spin system (HS Co^{2+}, d^7) in octahedral environment, the zero field perturbation splits the energy levels into two doublets, $|\pm 1/2\rangle$ and $|\pm 3/2\rangle$. Thus, the nature of the spectrum could be assigned to the transitions between the ground state Kramers doublet with anisotropic g-factor, which is assumed to originate from the involvement of an excited doublet with an effective spin of 3/2.[73] The expected effective g-factor for high-spin Co^{2+} is about 4.3 in ideal oxygen octahedral environment[73] or takes lower value when octahedron is distorted.

In order to estimate the main ESR parameters of the line we have fitted the experimental spectra by sum of two components corresponding to the principal values of the g-tensor in accordance with sum of two Lorentzian functions of the type:

DOI: 10.1039/C6DT00516K

$$\frac{dP}{dB} \propto \frac{d}{dB}\left[\frac{\Delta B}{\Delta B^2 + (B - B_r)^2} + \frac{\Delta B)}{\Delta B^2 + (B + B_r)^2}\right], \quad (4)$$

which takes into account two circular components of the exciting linearly polarized microwave field. Here *P* is the power absorbed in the ESR experiment, *B* is the magnetic field, B_r the resonance field, and ΔB is the linewidth. The result of fitting are shown by solid lines in Fig. 9. A representative example of the spectrum decomposition is given in upper part of Fig. 10 along with two resolved resonance modes denoted by dashed lines. The temperature dependences of the effective g-factor and linewidth derived from this fitting are shown in lower part of Fig. 10. The principal g-values of the anisotropic g-tensor at room temperature take $g_{||}$ = 2.87±0.02 and $g_{\perp}$ = 2.17±0.02 resulting in average g = 2.40±0.05, being in reasonable agreement with other related Co(II) compounds with six O^{2-} ions as the nearest neighbors of Co^{2+}.[74,75]

It was established, that at high temperatures (T > 150 K) the absorption is characterized by almost temperature independent values of the effective g-factor and the linewidth ΔB (Fig. 10). Then, the whole spectrum broadens and visible shift of the resonance field occurs upon lowering of the temperature, indicating a large pre-ordering magnetic effect in $Ag_3Co_2SbO_6$ in the wide *T*-range 25 – 150 K. The individual components shows different behaviour: ESR linewidth $\Delta B_{\perp}$ demonstrates just small increase below 125 K, while the temperature dependence of linewidth for $\Delta B_{||}$ component is more obvious. The latter one markedly increases with decreasing temperature below 150 K and passes through a smooth maximum at about 75 K. This behaviour can be phenomenologically explained in terms of a fluctuating internal field which add to the applied field altering the resonance condition, while at the same time slowing down of the fluctuation rate of this field may produce a progressive broadening of the resonance line as the temperature decreases. The occurrence of such fluctuating fields might be traced to the noticeable short-range correlations in the system, which are present at temperatures essentially higher the long-range order temperature. The difference in behaviour of $\Delta B_{||}(T)$ and $\Delta B_{\perp}(T)$ might tentatively indicate that the correlations in $Ag_3Co_2SbO_6$ are evolving in an anisotropic manner. Typically, ESR spectra tend to broaden monotonically upon lowering temperature as spin correlations develop. Nevertheless, the linewidth passes through a maximum and then varies very weakly upon approaching the Néel temperature. This may reflect the saturation of the spin correlation length and the depletion of the spin fluctuation density. Note, that the presence of strong short-range fluctuations is evident also from the static susceptibility data showing visible deviation from the Curie-Weiss law below the same temperature ~ 150 K (Fig. 5(a)).

Band structure calculations and analysis of the orbital structure.

The total and partial density of states of $Ag_3Co_2SbO_6$ obtained in the GGA+U calculations are presented in Fig. 11. One may

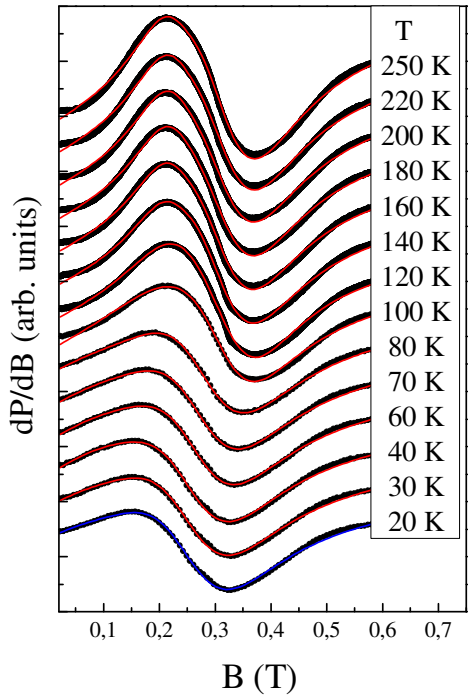

Fig. 9 Temperature evolution of the first derivative ESR absorption line for Ag3Co2SbO6: black points – experimental data, lines – fitting in accordance with sum of two components as described in the text.

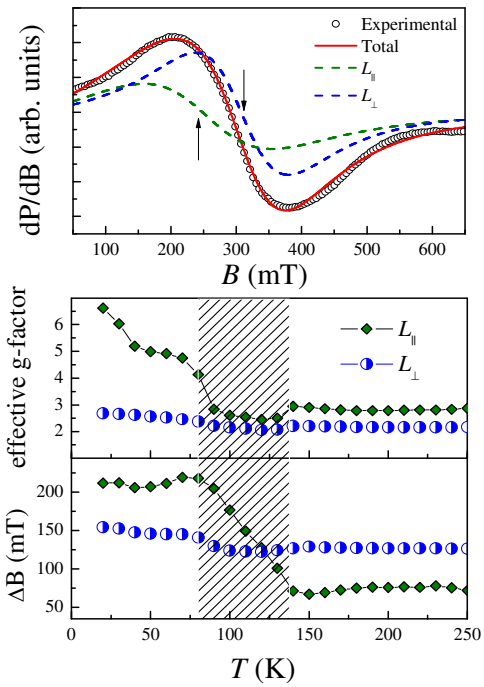

Fig. 10 Representative example of ESR spectra decomposition along with two modes (upper) and temperature dependence of g-values and ESR linewidth for two principal components of g-tensor (lower). The dashed lines show the individual Lorentzian fit components and the solid line is their sum.

View Article Online
DOI: 10.1039/C6DT00516K

see that for given values of U and J_H parameters this compound is insulating with the band gap ~1 eV. The top of the valence band is defined by O-p, while the bottom of the conduction band by the Ag-s,p,d and Co-d states. Spin moment on Co was found to be 2.7 μ_B, which is close to the ionic value for Co^{2+}, but reduced due to the hybridization, which is typical for transition metal compounds.

We calculated four magnetic configurations, which are shown in Fig. 1 of Ref. 76 in order to extract three exchange integrals: J_1^s, J_1^l, and J_2 in the *ab* plane. First two exchange parameters, J_1^s and J_1^l, are between nearest neighbors in the honeycomb plane; J_1^s is along the shortest Co-Co pathways (there are two such pairs in each hexagon as denoted by red bars in Fig. 3 and Fig. 12), while J_1^l characterizes magnetic coupling for long Co-Co pairs (4 bonds in each hexagon as denoted by yellow bars in Fig. 3). J_2 is the average exchange between next nearest neighbors in the hexagonal plane.

It was found that similarly to related honeycomb lattice antimonates $A_3Ni_2SbO_6$ (A = Li, Na)[76] the lowest total energy corresponds to the AFM zigzag state. It is important to mention that this type ordering has been recently evidenced for honeycomb-lattice delafossites $Cu_3Ni_2SbO_6$ and $Cu_3Co_2SbO_6$ as refined experimentally from low temperature neutron diffraction studies.[40,41] In $Ag_3Co_2SbO_6$ the exchange parameters were calculated to be J_1^s =28 K (AFM), J_1^l =-2 K (FM), and J_2=3 K (AFM). This is rather intriguing, that two nearest neighbor exchanges, J_1^s and J_1^l, are so different. Indeed, the difference in the Co-Co lengths is not so large: δr ~ 0.016 A. If one assumes that $J_1 \sim 2t^2/U$ and the *d-d* hopping *t* follows conventional Harrison's dependence $t_d \sim 1/r^5$ [77] (*r* here is the distance between Co), than this change in *r* would result only in 5% difference in the exchange. An account of the superexchange contribution and *r*-dependence of *p-d* hopping does not improve the situation considerably, so that the origin of the strong difference in nearest neighbor exchanges has to be due to some other mechanism.

In order to find this mechanism we analyzed the orbital structure. As it was mentioned above Co ions have octahedral surrounding in $Ag_3Co_2SbO_6$. Moreover, these octahedra turned out to be compressed, which results in a particular splitting of the Co 3*d* shell. If one would chose local coordinate system as shown in Fig. 12 (i.e. all axes are directed to the oxygens; *z*-axis is along the shortest Co-O bonds), than t_{2g} subband is split on lower lying in energy *xy* and higher *zx*/*yz* subbands. In the case of $3d^7$ configuration (Co^{2+}) this is the *zx*/*yz* subband, which turns out to be 3/4-filled and hence "magnetically active". This is the feature of the $Ag_3Co_2SbO_6$ crystal structure, that the shortest Co-O bonds are directed very differently in pairs of the CoO_6 octahedra forming short and long Co-Co nearest neighbor bonds. This leads to a specific orbital order, which in turn results in very different exchange parameters for these bonds. We used Linearized muffin-tin orbitals (LMTO) method[78] to plot the single half-filled t_{2g} orbital in the LDA+U calculation. This method is based on the atomic-like wave functions, which makes such a procedure straightforward (the same method was used previously, e.g. in $CaCrO_3$[79] and $NaMn_7O_{12}$[80]). The resulting orbital order is shown in Fig. 12. One may see that the single half-filled t_{2g} orbitals for two Co ions forming short (red in Figs. 3 and 12) Co-Co bonds are directed to each other (these are the *xz*+*yz* orbitals in the coordinate system with *z*-axis directed along short, (blue) Co-O bond and *x* and *y* axes pointing to oxygens forming common edge). Such an orbital pattern will result in AFM exchange via both direct and superexchange mechanisms. In contrast, if one considers long Co-Co bonds than it turns out that these half-filled *xz*+*yz* orbitals do not overlap with each other, i.e. direct AFM exchange via long Co-Co bonds is suppressed by this orbital order. Moreover, the superexchange via the same *p*-

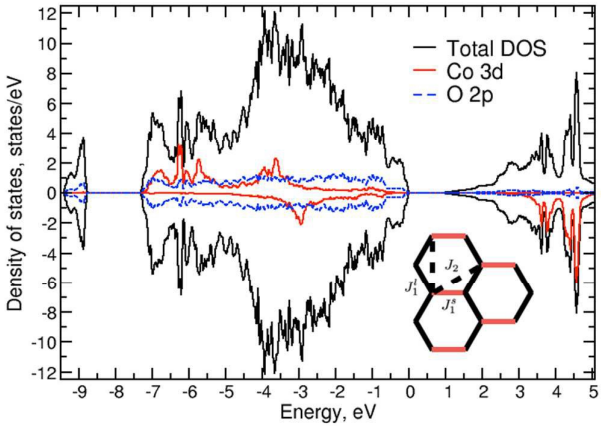

Fig. 11 Total and partial density of states for $Ag_3Co_2SbO_6$ as obtained in the GGA+U calculation for the AFM zigzag order. Total density of states is normalized per formula unit, while partial – per ion. Upper (lower) panel corresponds to spin majority (minority). The Fermi energy is set to zero. The inset shows how the exchange parameters are defined: J_1^l is between long (black) nearest neighbors, J_1^s is between short (red) nearest neighbors Co ions, J_2 is the average exchange between next nearest neighbors in the hexagonal plane.

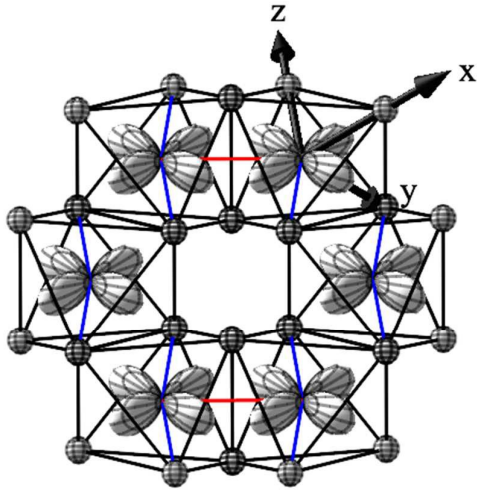

Fig. 12 The orbital order as obtained in the LDA+U calculations (in the LMTO). The single half-filled t_{2g} orbital of Co is shown. O ions are blue balls, short Co-Co bonds are painted in red, short Co-O bonds in blue. The AFM zigzag order is shown by green arrows. For one of the CoO_6octahedra the local coordinate system is presented.

DOI: 10.1039/C6DT00516K

orbital of oxygen is also impossible due to signs of the *p*- and *d*-wave functions. The superexchange via different *p*-obitals is possible, but it is usually small and FM.[81] Since *xy*-orbital on each Co is fully occupied the t_{2g}-e_g exchange is vanishingly small. The superexchange between e_g orbitals is also not operative in the common edge geometry.[81,82]

Thus, the analysis performed above shows that the orbital order realizing in $Ag_3Co_2SbO_6$ blocks AFM t_{2g}-t_{2g} exchange between part of the nearest neighbor Co ions. The situation here reminds $NaTiSi_2O_6$, where features of the crystal structure strongly affect the nearest neighbor exchange in such a way that half-filled *d*-orbitals in part of the metal-metal pairs turn out to be "parallel" to each other, but do not overlap and do not contribute to the exchange coupling.[81,83,84] The analysis of orbital structure in $Ag_3Co_2SbO_6$ fully agrees with estimations of the exchange integrals obtained with the use of the total energy calculations according to which there is only one strong exchange coupling in this system and this is the exchange corresponding to the shortest Co-Co bonds.

Magnetic phase diagram

Summarizing the data of thermodynamic studies, performed in the present work, the magnetic phase diagram for the new honeycomb lattice dellafossite $Ag_3Co_2SbO_6$ was constructed (Fig. 13). In zero magnetic field the paramagnetic phase is realized at temperatures higher than 21.2 K, while applying the magnetic field slightly shifts this phase boundary toward the lower temperatures, which is typical for antiferromagnets. It is also evident from the *B*-*T* diagram that one more magnetic phase (II) is induced by applying a magnetic field below T_N and probably associated with different mutual orientations of neighboring spins in honeycomb lattice. The quantum ground state of $Ag_3Co_2SbO_6$ was determined as zigzag antiferromagnetic state (I) exists below ~ 2.7 T.

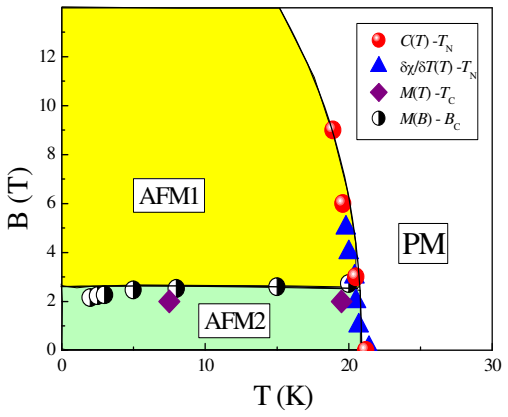

Fig. 13 Magnetic phase diagram for antimonate $Ag_3Co_2SbO_6$ as defined from thermodynamic (magnetization d*M*/d*T* and d*M*/d*B* and specific heat *C*(*T*)) measurements.

Conclusions

In conclusion, we have revised the crystal structure and for the first time investigated the magnetic properties of a quasi 2D honeycomb-lattice layered silver delafossite $Ag_3Co_2SbO_6$. The static magnetic susceptibility and specific heat data show the onset of antiferromagnetic order at T_N ~ 21.2 K. The entropy release occurs mainly at temperatures higher than T_N, indicating the presence of appreciable short-range correlations in the compound. The high-temperature magnetic susceptibility data exhibits Curie-Weiss behavior with a Weiss temperature Θ ~ –9 K that indicates a predominance of the antiferromagnetic coupling. ESR spectra in the paramagnetic phase show a broad anisotropic line attributed to Co^{2+} ions in distorted octahedral coordination characterized by the average g-factor g = 2.40±0.05. However, the distortion, broadening of the ESR absorption line and shift of the resonant field were found to take place below ~ 150 K, which imply complex spin dynamics and an extended region of short-range order correlations in this quasi 2D compound. The theoretical calculations show that the strongest exchange interaction is between the nearest neighbours, but this nearest neighbours exchange is essentially affected by a specific orbital structure, which suppresses antiferromagnetic exchange in four out of six (nearest neighbour) Co-Co pathways within the cobalt hexagon. It was also found that both ferromagnetic and antiferromagnetic intraplane exchange interactions are present on the honeycomb Co_2SbO_6 layers and the most favourable spin configuration model is weakly ferromagnetic chains, which are coupled via strong antiferromagnetic exchange resulting in overall zigzag AFM order in $Ag_3Co_2SbO_6$. We also found that the orbital degrees of freedom set up a hierarchy of the exchange interaction Ag3Co2SbO6, which makes delafossites, espesially those based on Co ions, important class of materials with the strong interplay between different degrees of freedom.

Acknowledgements

E.A.Z., V.B.N. and I.L.S. appreciate support from the Russian Foundation for Basic Research (grants 14-02-00245 and 11-03-01101). E.A.Z., S.V.S. and A.V.U. appreciate support from the Russian Foundation for Basic Research (grant 13-02-00374), S.V.S. and A.N.V. also acknowledge support from the FASO (theme "Electron" No. 01201463326) and Government of the Russian Federation, contract № 02.A03.21.0006. This work was supported in part from the Ministry of Education and Science of the Russian Federation in the framework of Increase Competitiveness Program of NUST «MISiS» (№ K2-2015-075). The work in Germany by M.A. was supported by the DFG Eigene Stelle MO 3014/1-1. The work of A.V.S. was supported by the FNRS projects, credit de demarrage U.Lg."

View Article Online
DOI: 10.1039/C6DT00516K

References

1 M.A. Marquardt, N.A. Ashmore, D.P. Cann, *Thin Solid Films*, 2006, **496**, 146; W.C. Sheets, E. Mugnier, A. Barnabé, T.J. Marks, and K.R. Poeppelmeier, *Chem. Mater.*, 2006, **18**, 7; R.D. Shannon, D.B. Rogers and C.T. Prewitt, *Inorg. Chem.*, 1971, **10**, 713.

2 S. Seki, Y. Onose and Y. Tokura, *Phys. Rev. Lett.*, 2008, **101**, 067204.

3 K. Kimura, H. Nakamura, S. Kimura, M. Hagiwara and T. Kimura, *Phys. Rev. Lett.*, 2009, **103**, 107201.

4 K. Kimura, H. Nakamura, K. Ohgushi and T. Kimura, *Phys. Rev. B*, 2008, **78**, 140401(R).

5 A. Vasiliev, O. Volkova, I. Presniakov, A. Baranov, G. Demazeau, J.M. Broto, M. Millot, N. Leps, R. Klingeler, B. Büchner, M.B. Stone and A. Zheludev, *J. Phys. Cond. Matter*, 2010, **22**, 016007.

6 N. Terada, D.D. Khalyavin, P. Manuel, Y. Tsujimoto, K. Knight, P.G. Radaelli, H.S. Suzuki and H. Kitazawa, *Phys. Rev. Lett.*, 2012, **109**, 097203.

7 T. Kimura, J. C. Lashley and A. P. Ramirez, *Phys. Rev. B*, 2006, **73**, 220401(R).

8 T. Nakajima, S. Mitsuda, K. Takahashi, M. Yamano, K. Masuda, H. Yamazaki, K. Prokes, K. Kiefer, S. Gerischer, N. Terada, H. Kitazawa, M. Matsuda, K. Kakurai, H. Kimura, Y. Noda, M. Soda, M. Matsuura and K. Hirota, *Phys. Rev. B*, 2009, **79**, 214423.

9 S. Kanetsuki, S. Mitsuda, T. Nakajima, D. Anazawa, H. A. Katori and K. Prokes, *J. Phys. Cond. Matter*, 2007, **19**, 145244.

10 S. Seki, Y. Yamasaki, Y. Shiomi, S. Iguchi, Y. Onose and Y. Tokura, *Phys. Rev. B*, 2007, **75**, 100403(R).

11 N. Terada, T. Nakajima, S. Mitsuda, H. Kitazawa, K. Kaneko and N. Metoki, *Phys. Rev. B*, 2008, **78**, 014101.

12 K. Singh, A. Maignan, C. Martin and C. Simon, *Chem. Mater.*, 2009, **21**, 5007.

13 S.V. Streltsov, A.I. Poteryaev and A.N. Rubtsov, *J. Phys. Cond. Matt.*, 2015, **27**, 165601.

14 M. Hemmida, H.-A. Krug von Nidda and A. Loidl, *J. Phys. Soc. Japn.*, 2011, **80**, 053707.

15 M. Poienar, C. Vecchini, G. Andr`e, A. Daoud-Aladine, I. Margiolaki, A. Maignan, A. Lappas, L. Chapon, M. Hervieu, F. Damay and C. Martin, *Chem. Mater.*, 2011, **23**, 85.

16 A.V. Ushakov, S.V. Streltsov,and D.I. Khomskii, *Phys. Rev. B*, 2014, **89**, 024406.

17 T. Okuda, T. Kishimoto, K. Uto, T. Hokazono, Y. Onose, Y. Tokura, R. Kajimoto and M. Matsuda, *J. Phys. Soc. Japn.*, 2009, **78**, 013604.

18 Z.Y. Meng, T.C. Lang, S. Wessel, F.F. Assaad and A. Muramatsu, *Nature*, 2010, **464**, 847.

19 Fa Wang, *Phys. Rev. B*, 2010, **82**, 024419.

20 B.K. Clark, D.A. Abanin and S.L. Sondhi, *Phys. Rev. Lett.*, 2011, **107**, 087204.

21 S.A.J. Kimber, I.I. Mazin, J. Shen, H.O. Jeschke, S.V. Streltsov, D.N. Argyriou, R. Valenti and D.I. Khomskii, *Phys. Rev. B*, 2014, **89**, 081408.

22 S.V Streltsov and D.I. Khomskii, *Phys. Rev. B*, 2014, **89**, 161112.

23 J.C. Wang, J. Terzic, T.F. Qi, F. Ye, S.J. Yuan, S. Aswartham, S.V. Streltsov, D.I. Khomskii, R.K. Kaul and G. Cao, *Phys. Rev. B*, 2014, **90**, 161110.

24 R. Ganesh, J. van den Brink and S. Nishimoto, Phys. Rev. Lett., 2013, **110**, 127203.

25 S. Streltsov, I.I. Mazin and K. Foyevtsova, *Phys. Rev. B*, 2015, **92**, 134408.

26 S. Pujari, K. Damle and F. Alet, *Phys. Rev. Lett.*, 2013, **111**, 087203.

27 Y. Zhong, Y.-F. Wang and H.-G. Luo, *Phys. Rev. B*, 2013, **88**, 045109.

28 A.G. Grushin, E.V. Castro, A. Cortijo, F. de Juan, M.A.H. Vozmediano and B. Valenzuela, *Phys. Rev. B*, 2013, **87**, 085136.

29 H. Zhang and C. A. Lamas, *Phys. Rev. B*, 2013, **87**, 024415.

30 R. Ganes, S. Nishimoto and J. van den Brink, *Phys. Rev. B*, 2013, **87**, 054413.

31 R. Nagarajan, S. Uma, M.K. Jayaraj, J. Tate and A.W. Sleight, *Solid State Sci.*, 2002, **4**, 787.

32 E. Climent-Pascual, P. Norby, N.H. Andersen, P.W. Stephens, H.W. Zandbergen, J. Larsen and R.J. Cava, *Inorg. Chem.*, 2012, **51**, 557.

33 J. Xu, A. Assoud, N. Soheinia, S. Derakhshan, H. L. Cuthbert, J.E. Greedan, M. H. Whangbo and H. Kleinke, *Inorg. Chem.*, 2005, **44**, 5042.

34 K. Morimoto, Y. Itoh, K. Yoshimura, M. Kato and K. Hirota, *J. Phys. Soc. Japn.*, 2006, **75**, 083709.

35 S. Derakhshan, H.L. Cuthbert, J.E. Greedan, B. Rahaman and T. Saha-Dasgupta, *Phys. Rev. B*, 2007, **76**, 104403.

36 Y. Miura, R. Hirai, Y. Kobayashi and M. Sato, *J. Phys. Soc. Japn.*, 2006, **75**, 084707.

37 Y. Miura, R. Hirai, T. Fujita, Y. Kobayashi and M. Sato, *J. Magn. Magn. Mater.*, 2007, **310**, e389.

38 Y. Miura, Y. Yasui, T. Moyoshi, M. Sato, K. Kakurai, *J. Phys. Soc. Japn.*, 2008, **77**, 104709.

39 C.N. Kuo, T.S. Jian and C.S. Lue, *J. Alloys Comp.*, 2012, **531**, 1.

40 J.H. Roudebush, N.H. Andersen, R. Ramlau, V.O. Garlea, R. Toft-Petersen, P. Norby, R. Schneider, J.N. Hay and R.J. Cava, *Inorg. Chem.*, 2013, **52**, 6083.

41 J.H. Roudebush, G. Sahasrabudhe, S.L. Bergman and R.J. Cava, *Inorg. Chem.*, 2015, **54**, 3203.

42 C. Linke and M. Jansen, *Z. anorg. allgem. Chem.*, 1997, **623**, 1441.

43 T. Oku, A. Carlsson, J.-O. Bovin, C. Svensson, L.R. Wallenberg, C. Linke and M. Jansen, *Acta Cryst. B*, 2000, **56**, 363.

44 V.B. Nalbandyan, *Russ. J. Inorg. Chem.*, 2000, **45**, 1652.

45 Y. Hosogi, H. Kato and A. Kudo, *J. Mater. Chem.*, 2008, **18**, 647.

46 V.V. Politaev, V.B. Nalbandyan, A.A. Petrenko, I.L. Shukaev, V.A. Volotchaev and B.S. Medvedev, *J. Solid State Chem.*, 2010, **183**, 684.

47 S.A.J. Kimber, C.D. Ling, D.J.P. Morris, A. Chemseddine, P.F. Henry and D.N. Argyriou, *J. Mater. Chem.*, 2010, **20**, 8021.

48 K. Ramesha, A.S. Prakash, M. Sathiya, G. Madras and A.K. Shukla, *Mater. Sci. Eng. B*, 2011, **176**, 141.

49 V. Todorova, A. Leineweber, L. Kienle, V. Duppel and M. Jansen, *J. Solid State Chem.*, 2011, **184**, 1112.

50 R. Berthelot, W. Schmidt, S. Muir, J. Eilertsen, L. Etienne, A.W. Sleight and M.A. Subramanian, *Inorg. Chem.*, 2012, **51**, 5377.

51 V.V. Politaev and V.B. Nalbandyan, *Solid State Sci.*, 2009, **11**, 144.

52 V. Kumar, N. Bhardwaj, N. Tomar, V. Thakral and S. Uma, *Inorg. Chem.*, 2012, **51**, 10471.

53 N. Bhardwaj, A. Gupta and S. Uma, *Dalton Trans.*, 2014, **43**, 12050.

54 A. C. Larson, R. B Von Dreele, General Structure Analysis System (GSAS); *Los Alamos National Laboratory Report LAUR* 86-748; Los Alamos National Laboratory: Los Alamos, NM, 2004.

55 B. H. Toby, *J. Appl. Crystallogr.*, 2001, **34**, 210.

56 A.I. Liechtenstein, V.I. Anisimov and J. Zaanen, *Phys. Rev. B*, 1995, **52**, 5467.

57 P. Blaha, K. Schwarz, G. K. H. Madsen, D. Kvasnicka and J. Luitz, *WIEN2k, An Augmented Plane Wave + Local Orbitals Program for Calculating Crystal Properties*, Techn. Universität Wien, Wien, 2001.

58 J.P. Perdew, K. Burke and M. Ernzerhof, *Phys. Rev. Lett.*, 1996, **77**, 3865.
59 M.M. Markina, B.V Mill, E.A. Zvereva, A.V Ushakov, S.V Streltsov and A.N. Vasiliev, *Phys. Rev. B*, 2014, **89**, 104409.
60 I.P. Muthuselvam, R. Sankar, A.V Ushakov, G.N. Rao, S.V Streltsov and F.C. Chou, *Phys. Rev. B*, 2014, **90**, 174430.
61 L. Viciu, Q. Huang, E. Morosan, H.W. Zandbergen, N.I. Greenbaum, T. McQueen and R.J. Cava, *J. Solid State Chem.*, 2007, **180**, 1060.
62 C. Greaves and S.M.A. Katib, *Mat. Res. Bull.*, 1990, **25**, 1175.
63 E.A. Zvereva, M.A. Evstigneeva, V.B. Nalbandyan, O.A. Savelieva, S.A. Ibragimov, O.S. Volkova, L.I. Medvedeva, A.N. Vasiliev, R. Klingeler and B. Buechner, *Dalton Trans.*, 2012, **41**, 572.
64 R.V. Panin, N.R. Khasanova, A.M. Abakumov, E.V. Antipov, G. Van Tendeloo and W. Schnelle, *J. Solid State Chem.*, 2007, **180**, 1566.
65 Y. Singh and P. Gegenwart, *Phys. Rev. B*, 2010, **82**, 064412.
66 J. Ma, S.-H. Bo, L. Wu, Y. Zhu, C.P. Grey and P.G. Khalifah, *Chem. Mater.*, 2015, **27**, 2387.
67 E.A. Zvereva, O.A. Savelieva, Ya.D. Titov, M.A. Evstigneeva, V.B. Nalbandyan, C.N. Kao, J.-Y. Lin, I.A. Presniakov, A.V. Sobolev, S.A. Ibragimov, M. Abdel-Hafiez, Yu. Krupskaya, C. Jähne, G. Tan, R. Klingeler, B. Büchner and A.N. Vasiliev, *Dalton Trans.*, 2013, **42**, 1550.
68 M.E. Fisher, *Proc. Roy. Soc.* (London), 1960, **A 254**, 66.
69 M.E. Fisher, *Phil. Mag.*, 1962, **7**, 1731.
70 R.L. Carlin, *Magnetochemistry*, Springer-Verlag, Berlin Heidelberg New York Tokyo, 1986.
71 A. Tari, *The specific heat of matter at low temperature*, Imperial College Press, London, 2003.
72 L.J. de Jongh and A.R. Miedema, *Adv. Phys.*, 1974, **23**, 1.
73 A. Abragam and B. Bleaney, *EPR of Transition Ions*, Clarendon, Oxford, 1970; A. Abragam and M.H.L. Pryce, *Proc. Roy. Soc.* (London), 1951, **A 200**, 173.
74 J.J. Borras-Almenar, E. Coronado, D. Gatteschi, and C. Zanchini, *Inorg. Chem.*, 1992, **31**, 294
75 J.M. Rojo, J.L. Mesa, J.L. Pizarro, L. Lezama, M.I. Arriortua, and T. Rojo, *J. Solid State Chem.*, 1997, **132**, 107.
76 E.A. Zvereva, M.I. Stratan, Y.A. Ovchenkov, V.B. Nalbandyan, J.-Y. Lin, E.L. Vavilova, M.F. Iakovleva, M. Abdel-Hafiez, A.V. Silhanek, X.-J. Chen, A. Stroppa, S. Picozzi, H.O. Jeschke, R. Valentí and A.N. Vasiliev, *Phys. Rev. B*, 2015, **92**, 144401.
77 W.A. Harrison, *Elementary Electronic Structure*, World Scientific, Singapore, 1999.
78 O.K. Andersen and O. Jepsen, *Phys. Rev. Lett.*, 1984, **53**, 2571.
79 S.V. Streltsov, M.A. Korotin, V.I. Anisimov and D.I. Khomskii, *Phys. Rev. B*, 2008, **78**, 054425.
80 S.V. Streltsov and D.I. Khomskii, *Phys. Rev. B*, 2014, **89**, 201115.
81 S.V. Streltsov and D.I. Khomskii, *Phys. Rev. B*, 2008, **77**, 064405.
82 J.B. Goodenough, *Magnetism and the Chemical Bond*, (Interscience publishers, New York-London, 1963.
83 S.V. Streltsov, O.A. Popova, D.I. Khomskii, *Phys. Rev. Lett.*, 2006, **96**, 249701.
84 M. Isobe, E. Ninomiya, A.N. Vasil'ev, and Y. Ueda, *J. Phys. Soc. Japn.*, 2002, **71**, 1423.

View Article Online
DOI: 10.1039/C6DT00516K

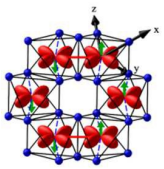

Revised crystal structure, static and dynamic magnetic properties and GGA+U calculations for layered honeycomb-lattice silver delafossite $Ag_3Co_2SbO_6$ are reported.